Reconnection Dynamics with Secondary Tearing Instability in Compressible Hall Plasmas

Z. W. Ma*, L. C. Wang, L. J. Li

Institute for Fusion Theory and Simulation, Zhejiang University, Hangzhou 310027, China.

Abstract: The dynamics of a secondary tearing instability is systematically investigated based on compressible Hall MHD. It is found that in the early nonlinear phase of magnetic reconnection before onset of the secondary tearing instability, the geometry of the magnetic field in the reconnection region tends to form a Y-type structure in a weak Hall regime, instead of an X-type structure in a strong Hall regime. A new scaling law is found that the maximum reconnection rate in the early nonlinear stage is proportional to the square of the ion inertial length ($\gamma \propto d_i^2$) in the weak Hall regime. In the late nonlinear phase, the thin elongated current sheet associated with the Y-type geometry of the magnetic field breaks up to form a magnetic island due to a secondary tearing instability. After the onset of the secondary tearing mode, the reconnection rate are substantially boosted by the formation of the X-type geometries of magnetic field in the reconnection regions. With a strong Hall effect, the maximum reconnection rate linearly increases with the increase of the ion inertial length ($\gamma \propto d_i$).

Keywords: Magnetic reconnection, tearing instability, secondary tearing mode, Hall MHD

*) Corresponding author: zwma@zju.edu.cn

1. Introduction

Magnetic reconnection is an effective mechanism to convert magnetic energy to kinetic and thermal energies and also leads to exchange of mass, momentum, energy between the two sides of the central current sheet. Magnetic reconnection is often cited as an efficient mechanism for many eruptive physical phenomena such as flares in the solar corona, substorms in the Earth's magnetosphere, and sawtooth oscillations in Tokamaks [*Sweet*, 1958; *Parker*, 1963; Yamada *et al*., 2010; Biskamp, 2000]. In order to use magnetic reconnection to explain observational phenomena [e.g. Nagai et al., 2012; Xiao et al., 2007; Kopp and Pneuman, 1976], the time scale of magnetic reconnection becomes a crucial issue, i.e., the reconnection time scale must be much faster than the diffusion time scale.

The first well known steady state models of reconnection, the Sweet-Parker model [Sweet, 1958; Parker 1957], states that the geometry of the reconnection layer has a Y-type structure [Syrovatskii, 1971] and its length is of the order of the system size. For high-S plasmas, however, the reconnection time scale $\tau_{sp} = \left(\tau_A \tau_R\right)^{1/2} = S^{1/2}\tau_A$ for Sweet-Parker model is too long to explain fast reconnection phenomena such as solar flare. The Petschek model [Petschek, 1964] replaces by an X-type structure from the Y-type geometry in the Sweet-Parker model and gives much faster reconnection time scale. Nevertheless, this model is not realizable in high-S plasmas, unless the resistivity is locally and strongly enhanced at the X-point. In the absence of such anomalous enhancement, the reconnection layer evolves dynamically to form Y-points and realize a Sweet-Parker regime [Ma et al., 1995].

In the reality, reconnection process, in general, is not steady-state, such as sawtooth oscillations in Tokamaks, magnetospheric substorms and solar flares. Magnetic reconnection is usually driven by external forces. Dynamic process of externally driven magnetic reconnection, which is characterized by the formation of near-singular current sheets in a finite time, exhibits a sudden change of the reconnection rate after the magnetic configuration evolves slowly for a long period of time. Analytical and simulation results based on the resistive magnetohydrodynamic (MHD) model have already been obtained [Wang et al., 1996].

In high-S plasmas, when the width of the thin current sheet (Δ_η) satisfies $c/\omega_{pe} \ll \Delta_\eta \ll c/\omega_{pi}$ (or $\sqrt{\beta}c/\omega_{pi}$ if there is a guide field), "collisionless" terms in the generalized Ohm's law cannot be ignored, which forms the so-called Hall MHD Model. A scaling analysis of the forced reconnection within the framework of the Hall MHD has been given by Wang et al. [2001]. This scaling law was confirmed by a later work [Wang et al., 2006]. In the regime with weak Hall effects, a so-called secondary tearing mode rises up, which has been presented by Zhang and Ma [2009] in their double tearing investigation. Also, a scaling law, which describes the relationship between the Lundquist number and the reconnection rate for the most rapidly growing plasmoid instability, has been obtained by Bhattacharjee et al. [2009]. And several subsequent works investigated more deeply on plasmoid scaling [e.g. Huang and Bhattacharjee, 2010; Huang et al., 2013].

In this paper, we will quantitatively examine the formation and evolution process of secondary tearing mode with different initial profile of magnetic field and plasma density. Similar initial profile has already been used in the Ma and Feng's work [2008] that mainly focused on the generation of Hall electric field and net charge associated with magnetic reconnection under the fixed ion inertial length. The time scales of the maximum reconnection rates associated with the secondary tearing mode will present under different initial profiles of the magnetic field and plasma density. A new scaling law is found that the maximum reconnection rate before the onset of the secondary tearing instability is proportional to the square of the ion inertial length, i.e., $\gamma \propto d_i^2$. However, it should be noted the geometry of the reconnection region remains a Y-type structure as in the Sweet-Parker mode even if the Hall effect still have a crucial influence on the reconnection rate at the low level.

The layout of this paper is given as follows. In Section 2, Hall MHD equations and numerical model are presented. Section 3 gives Hall MHD simulation results from symmetric magnetic field and uniform plasma density, while Section 4 provides several cases with asymmetric magnetic field or non-uniform plasma density profiles. Summary and discussion are placed in Section 5.

2. Equations and Numerical Model

The compressible Hall MHD model is employed to investigate the tearing mode dynamics in the process of magnetic reconnection. Resistivity is assumed to be uniform. Our simulations are conducted in the Cartesian coordinate system. The variation of all variables in the y-direction is assumed to be ignored; that is $\partial/\partial y=0$ for all the time. The magnetic field is given with the form $\mathbf{B}=\hat{y}\times\nabla\psi+B_y y$. The compressible Hall MHD equations employed in our simulations are as follows

$$\frac{\partial\rho}{\partial t}=-\nabla\cdot(\rho\mathbf{v}) \qquad (1)$$

$$\frac{\partial(\rho\mathbf{v})}{\partial t}=-\nabla\cdot[\rho\mathbf{vv}+(p+B^2/2)\mathbf{I}-\mathbf{BB}] \qquad (2)$$

$$\frac{\partial\psi}{\partial t}=-\mathbf{v}\cdot\nabla\psi+J_y/S+d_i(\mathbf{J}\times\mathbf{B})_y/\rho \qquad (3)$$

$$\frac{\partial B_y}{\partial t}=-\nabla\cdot(B_y\mathbf{v})+\mathbf{B}\cdot\nabla v_y+\nabla^2 B_y/S$$

$$-d_i\{\nabla\times[(\mathbf{J}\times\mathbf{B}-\nabla p)/\rho]\}_y \qquad (4)$$

$$\frac{\partial p}{\partial t}=-\nabla\cdot(p\mathbf{v})-(\gamma-1)p\nabla\cdot\mathbf{v}+J^2/S \qquad (5)$$

where $\mathbf{v}$, $\mathbf{B}$, $\mathbf{J}$, ψ, ρ, p, $\mathbf{I}$ are plasma velocity, magnetic field, current density, flux function, plasma density, thermal pressure, and unit tensor, respectively. $\gamma(=5/3)$ is the ratio of specific heats of plasma. All variables are normalized as follows: $\mathbf{B}/B_0\to\mathbf{B}$, $\mathbf{x}/a\to\mathbf{x}$, $t/\tau_A\to t$, $v/v_A\to v$, $\psi/(B_0 a)\to\psi$, $\rho/\rho_0\to\rho$, $p/(B_0^2/4\pi)\to p$, where $\tau_A=a/v_A$ is the Alfvénic time, $v_A=B_0/(4\pi\rho)^{1/2}$ is the Alfvénic speed, $a=\lambda_B$ and λ_B is the half width of initial current sheet. $S=\tau_R/\tau_A$ is the Lundquist number, where $\tau_R=4\pi a^2/\eta c^2$, c is the speed of light, η is the resistivity. d_i is the ion inertial length. The value of d_i can be used to represent the intensity of the Hall effects.

Equations above are solved with fourth-order Runge-Kutta method in time and fourth-order finite difference method in space. System size is chosen as $L_x = [-32, 32]$, $L_z = [-16,16]$, with 401×501 grid points which are nonuniform in both the *x* and *z* directions. Period boundary condition is imposed at $x = \pm L_x$ and free boundary condition, i.e., $\partial / \partial z = 0$ for all variables, is used at $z = \pm L_z$. The initial equilibrium is force-balanced. Thermal pressure is obtained by solving equilibrium equation:

$$p = (1+\beta)B_0^2 / 2 - B^2 / 2 \qquad (6)$$

where β is the asymptotic plasma beta. Initial magnetic field is given as:

$$\boldsymbol{B} = (-B_1 + B_0 \tanh(z / \lambda_B))\hat{\boldsymbol{x}} \qquad (7)$$

where λ_B is the half thickness of the current sheet, and is set to be 1.0 as a constant. B_0 is the initial asymptotic magnetic field strength, offset by $-B_1$, which is used to introduce asymmetric magnetic field. Other components of magnetic field are chosen to be zero at the initial state; that is $B_y = B_z = 0$. Initial plasma velocity is set to be zero, i.e. $v_x = v_y = v_z = 0$. In the present paper, we set $S = 1000$ for all cases.

The tearing mode is initially triggered by a small magnetic perturbation given by

$$\delta\psi = \delta\psi_0 \cos(\pi x / L_x)\cos(\pi z / 2L_z) \qquad (9)$$

where $\delta\psi_0 = 0.25$, which is chosen relatively large so that the system can attain a fast magnetic reconnection process [Ma and Bhattacharjee, 2001].

3. Simulation results with symmetric magnetic field and uniform plasma density

In our simulation, the magnetic reconnection rate γ can be calculated using the following method [Ma and Bhattacharjee, 2001]:

$$\gamma = \frac{\partial}{\partial t}\psi_r(t) \tag{10}$$

where the flux function ψ_r is collected at the reconnection point .

In this section, we choose symmetric plasma density and magnetic field condition, i.e., $B_0 = 1.0$, $B_1 = 0$ and the constant plasma density $\rho = 1.5$.

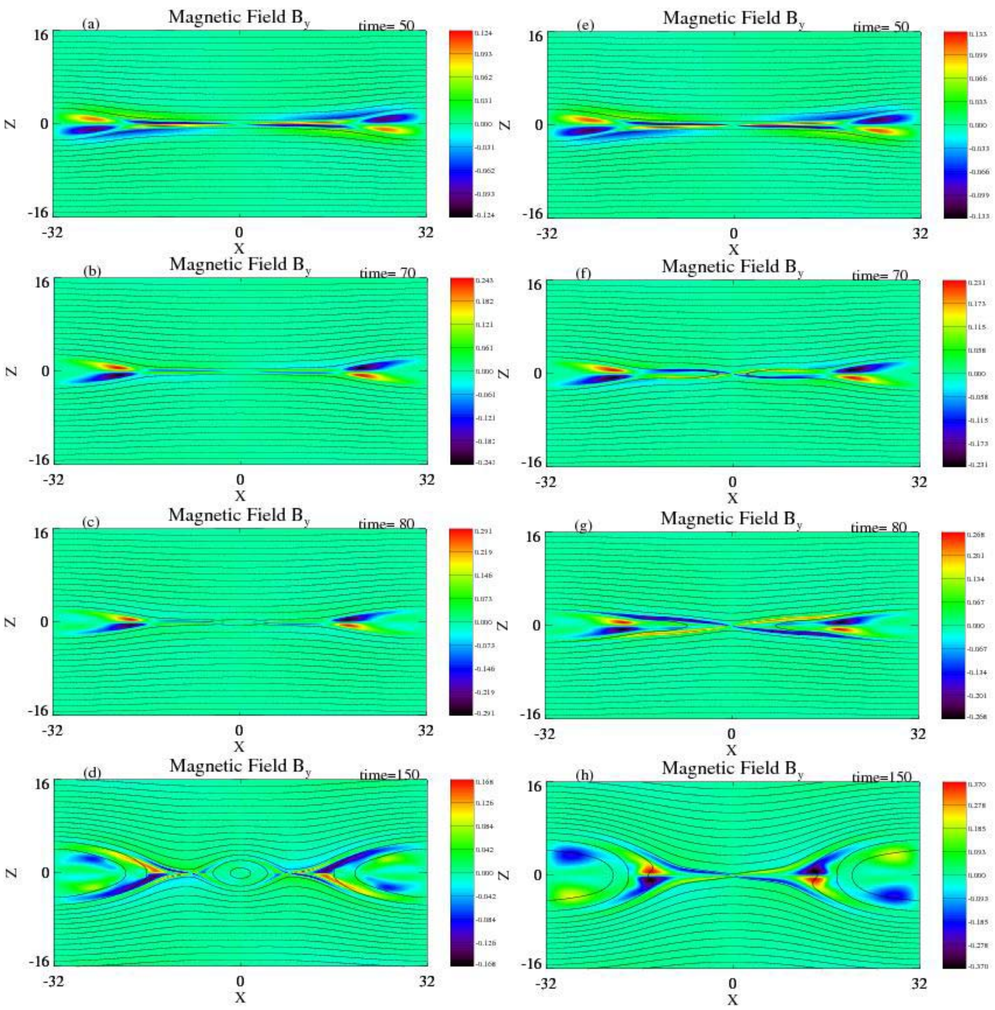

Figure 1. Contour images of B_y with magnetic field lines for $d_i = 0.5$ (left column) and $d_i = 0.6$ (right column) at t=50, 70, 80, 150.

Figure 1 shows several snapshots of the contour image plots of the guiding field component B_y with magnetic field lines for the cases $d_i = 0.5$ and $d_i = 0.6$. It is clearly shown that in the early phase of the magnetic reconnection, the geometry of magnetic field as well as the magnitudes and structures of the guiding field B_y are quite similar for the two cases as shown in Figures 1a and 1e because the Hall effect can be ignorable. After that, the reconnection dynamics of the two cases exhibit quite different scenarios. For the smaller d_i case, the reconnection region becomes further thin and elongated, and form a Y-type structure (Figure 1b). At the late stage t=80, the thin elongated current sheet breaks-up to form a magnetic island due to the secondary tearing instability (Figure 1c). The magnetic island further grows to a larger size (Figure 1d). For the larger d_i case, the reconnection region shrinks to form an X-type structure (Figure 1f). This X-type structure remains unchanged until the end of the simulation. There is no secondary tearing mode observed for the larger d_i case.

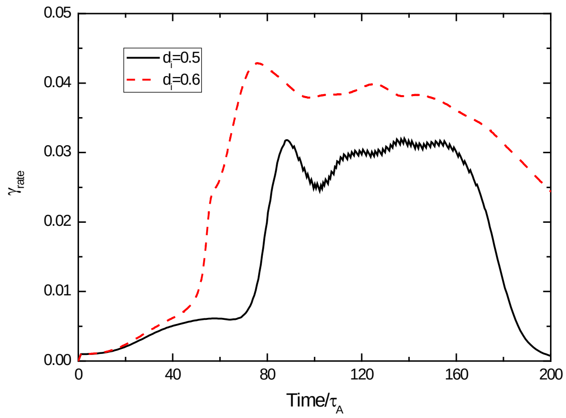

Figure 2. The time evolutions of the reconnection rates for $d_i = 0.5$ (the solid line) and $d_i = 0.6$ (the dashed line).

From the geometries of the magnetic field in Figure 1, we can separate the whole reconnection process into the reconnection stages before and after the onset of the secondary tearing instability for the smaller d_i regime. It is believed that there are double peaks of the reconnection rate associated with two different reconnection stages for the smaller d_i regime while there is only single peak of the reconnection rate for the larger d_i regime. The time evolutions of the reconnection rates are shown in Figure 2. Indeed, there exist two different reconnection stages for the smaller d_i regime. In the first stage, the thickness of the reconnection layer is not thin enough so that the reconnection dynamics are not mainly controlled by the Hall effect. After the onset of the secondary tearing instability, the Hall term in the generalized Ohm's law gradually becomes very important and the two reconnection regions exhibit the

X-type structure. Therefore, it is why the reconnection rate shows a bursty enhancement after the onset of the secondary tearing instability for the weak Hall regime. The reconnection rate in the second peak, resulted from the secondary tearing instability, increases more than five times of the reconnection rate in the first peak. The enhancement of the reconnection rate is rather lower in this Hall MHD model than in the resistive MHD model with a high Lundquist number [Bhattacharjee et al.; 2009]. They found that the averaged reconnection rate associated with the onset of the secondary tearing instability exceeds the Sweet-Parker rate by nearly an order of magnitude after the onset of secondary tearing mode. The main reason for the weakly boosting effect of the reconnection rate in the Hall MHD model is that we have a higher reconnection rate resulted from weak contribution of the Hall effect in the first stage for the small d_i.

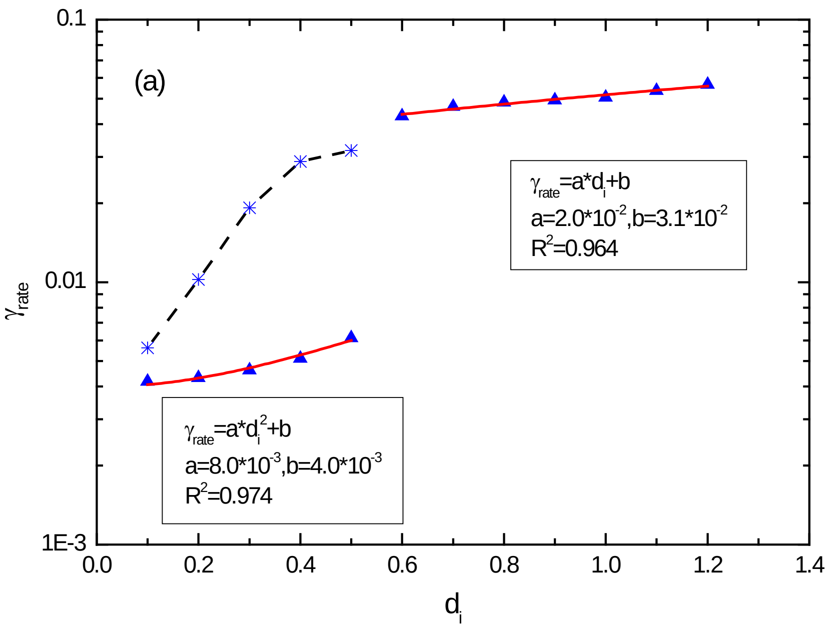

Figure 3. Summary of all peak reconnection rates for different d_i. The symbols "triangular" and "star" indicate the peak reconnection rates before and after the onset of secondary tearing instability.

Figure 3 shows the summary of all peak reconnection rates for different d_i. The peaks of the reconnection rates in the period with only one reconnection point existed in the simulation domain appear a large jump between the small and large d_i regimes as indicated by the solid lines. The critical value of d_i for the large jump of the reconnection rate is in between 0.5 and 0.6. Therefore, it could be argued that strong Hall effects for $d_i > 0.6$ in our model will lead to fast magnetic reconnection due to an X-type reconnection geometry without other secondary effects. For $d_i < 0.6$, fast magnetic reconnection can be achieved only through combination with the onset of the secondary tearing instability.

In order to examine the scaling law between the peak reconnection rate and the ion inertial length, the best fitting lines (the solid lines) are also given in Figure 3. For the small d_i regime, it is indicated that the first peak maximum reconnection rate before the onset of the secondary tearing instability is proportional to the square of the ion inertial length, i.e., $\gamma \propto d_i^2$. It is suggested that in the first stage, the Hall effect still have a crucial influence on the reconnection rate at the low level even if the geometry of the reconnection region exhibits a Y-type structure as in the Sweet-Parker mode. After the onset of the secondary tearing mode, the reconnection rate rises up dramatically, which is quite similar with the results from the resistive MHD model with a high Lundquist number [Bhattacharjee et al., 2009]. Although the onset of the secondary tearing mode causes much higher reconnection rate, the maximum reconnection rate in this phase still lies below that for the cases with a large d_i. For the cases with the large d_i, the maximum reconnection rate increases linearly as the ion inertial length increases, which shows a nice straight line fitting, i.e., $\gamma \propto d_i$.

4. Hall MHD simulation with asymmetric magnetic field or non-uniform plasma density

In the section, we investigate whether reconnection dynamics are affected by non-uniform density or asymmetric magnetic field. First, we consider the cases with the uniform plasma density and asymmetric magnetic field, i.e., $\rho = 1.5$ and $B_x(z) = -0.5 + 1.5\tanh(z)$. Figure 4 shows several snapshots of the contour image plots of the guiding field component B_y with magnetic field lines for the cases

$d_i = 0.6$ and $d_i = 0.7$. In the early phase of the magnetic reconnection, the geometry of magnetic field as well as the magnitudes and structures of the guiding field B_y are quite similar for the two cases as shown in Figures 4a and 4d. The asymmetric magnetic field leads to breaking-up the quadrupole symmetry of the guiding fields which are much larger in the weak field side than the strong field side. At time=50, the reconnection dynamics exhibit quite different. the thin elongated current sheet associated with the Y-type geometry of the magnetic field breaks-up to form a magnetic island due to the onset of the secondary tearing instability (Figure 4b). The magnetic island continuously grows to a larger size (Figure 4c). For the larger d_i case, the reconnection region shrinks to form an X-type structure (Figure 4e). This X-type structure remains unchanged until the end of the simulation (Figure 4f). There is also no secondary tearing mode observed for the larger d_i case. The guiding field exhibits a strong asymmetric and complicated distribution.

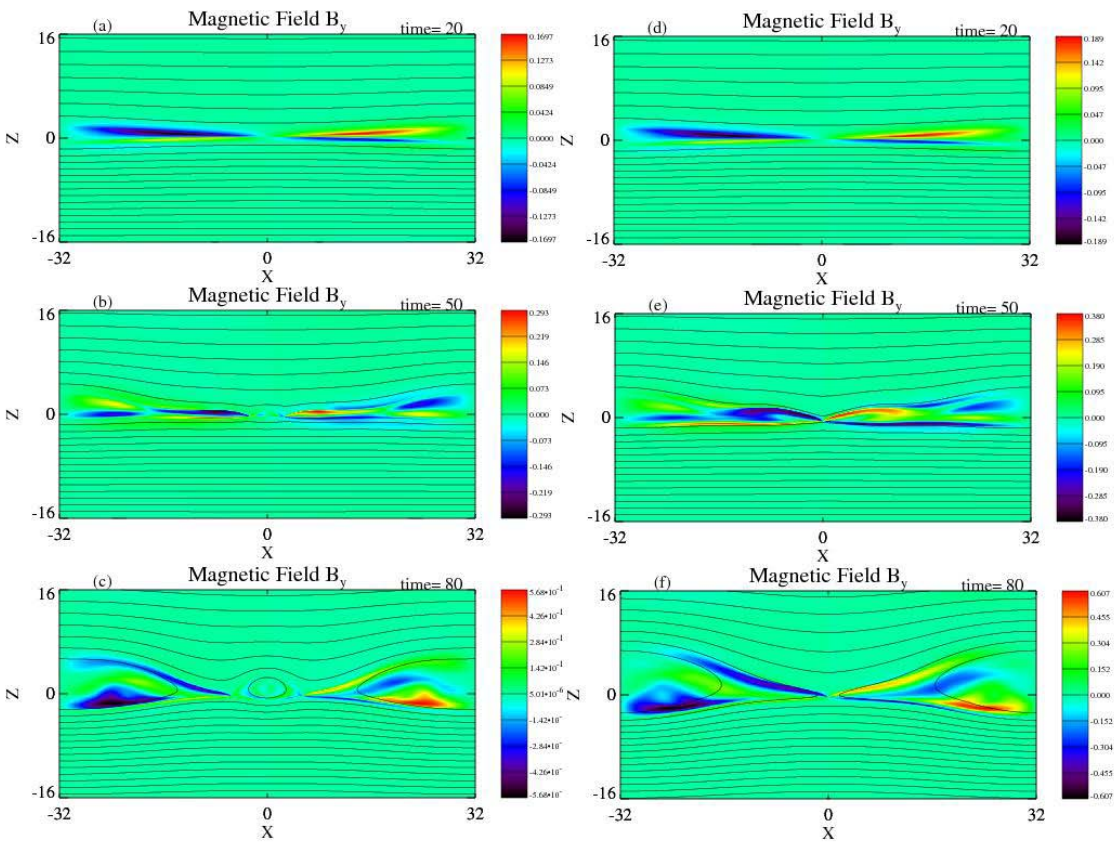

Figure 4. Contour image of B_y with magnetic field lines for $d_i = 0.6$ (left column) and $d_i = 0.7$ (right column) at *t*=20, 50, 80.

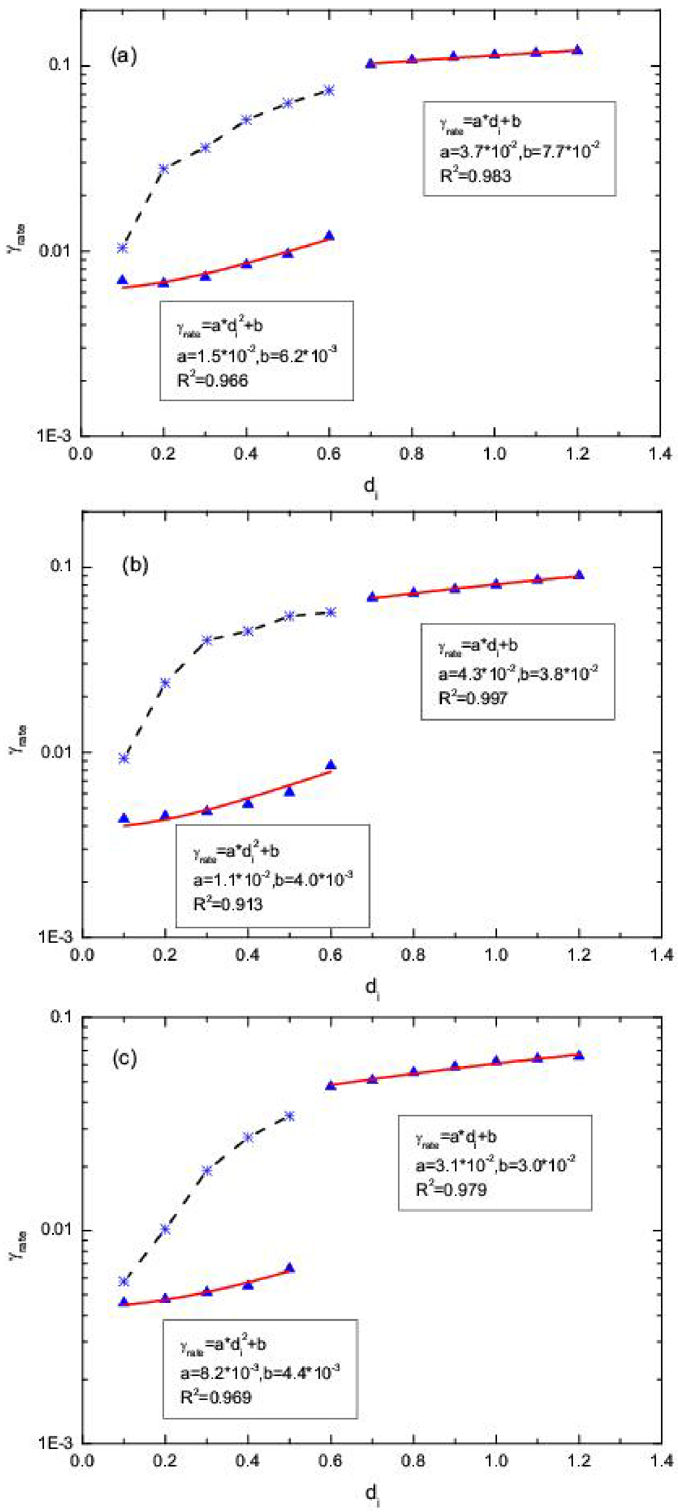

Figure 5. Dependence of peak reconnection rates on the ion inertial lengths d_i for three different initial profiles of the magnetic field and the plasma density. The symbols "triangular" and "star" indicate the peak reconnection rates before and after the onset of the secondary tearing instability.

Figure 5 shows the dependence of peak reconnection rates on the ion inertial lengths d_i for three different initial profiles of the magnetic field and the plasma density (a) $\rho = 1.5$ and $B_x(z) = -0.5 + 1.5\tanh(z)$, (b) $\rho = 0.8 + 0.7/\cosh^2(\mathrm{z})$ and $B_x(z) = \tanh(z)$, and (c) $\rho = 1.5 + 0.7\tanh(z)$ and $B_x(z) = \tanh(z)$. For all three different initial profiles, the peaks of the reconnection rates in the first stage also exist large jumps between the small and large d_i regimes as indicated by the solid lines. The critical values of d_i for the large jump of the reconnection rate only have slight differences. For the small d_i regime, magnetic reconnection is boosted due to the onset of the secondary tearing instability. The different initial profiles of the magnetic field and plasma density give the same scaling law between the peak reconnection rate and the ion inertial length indicated by the best fitting lines (the solid lines) in Figure 5. For the small d_i regime, the first peak maximum reconnection rate before the onset of the secondary tearing instability is proportional to the square of the ion inertial length, i.e., $\gamma \propto d_i^2$. For the large d_i, the maximum reconnection rate increases linearly as the ion inertial length increases, i.e., $\gamma \propto d_i$.

5. Summary and Discussions

Spontaneous reconnection dynamics with different initial profiles of the magnetic field and the plasma density are systematically investigated using compressible Hall MHD model. It is found that in the weak Hall regime, the whole reconnection process can be separated into the reconnection stages before and after the onset of the secondary tearing instability. In the first stage, both the Hall term and the resistive term in the generalized Ohm's law control the reconnection dynamics. A new scaling law is found that the maximum reconnection rate before the onset of the secondary tearing instability is proportional to the square of the ion inertial length, i.e., $\gamma \propto d_i^2$. However, it should be noted the geometry of the reconnection region remains a Y-type structure as in the Sweet-Parker mode even if the Hall effect still have a crucial influence on the reconnection rate at the low level. After the onset of the secondary tearing instability, the Hall term in the generalized Ohm's law gradually becomes very important and the geometries of the two reconnection regions exhibit the X-type structure, which suggests that the dynamics of magnetic reconnection is fully controlled by the Hall effect and the thickness of the reconnection layer goes well down below the ion inertial length. The reconnection rate shows a bursty enhancement for the weak Hall regime. The second maximum reconnection rate triggered by the secondary tearing instability increases more than five times of the first maximum reconnection rate. There is no obvious scaling law for the second maximum reconnection rate.

With a strong Hall regime, the maximum reconnection rate linearly increases with the increase of the ion inertial length, i.e., $\gamma \propto d_i$, which is different from the scaling law $\gamma \propto d_i^{1/2}$ for the driving reconnection [Wang et al., 2001].

Acknowledgement

This work is supported by the National Natural Science Foundation of China under Grant No. 11175156 and 41074105, the China ITER Program under Grant No. 2013GB104004 and 2013GB111004

References

Bhattacharjee, A., Y. M. Huang, H, Yang, B. Rogers (2009), Fast reconnection in high-Lundquist-number plasmas due to the plasmoid Instability, Physics of Plasmas 16, 112102.

Huang, Y. M., A. Bhattacharjee (2010), Scaling laws of resistive magnetohydrodynamic reconnection in the high-Lundquist-number, plasmoid-unstable regime, Physics of Plasmas 17, 62104.

Huang, Y. M., A. Bhattacharjee, T. G. Forbes (2013), Magnetic reconnection mediated by hyper-resistive plasmoid instability, Physics of Plasmas 20, 82131.

Kopp, R. A. and G. W. Pneuman (1976), Magnetic reconnection in the corona and the loop prominence phenomenon, Solar Physics 50, 85.

Ma, Z. W., A. Bhattacharjee (2001), Hall magnetohydrodynamic reconnection: The

Geospace Environment Modeling challenge, Journal of Geophysical Research 106, 3773.

Ma, Z. W., S. L. Feng (2008), Generation of Electric Field and Net Charge in Hall Reconnection, Chinese Physics Letters 25, 2934.

Ma, Z. W., X. G. Wang, A. Bhattacharjee (1995), Growth, sudden enhancement, and relaxation of current sheets in the magnetotail: Two-dimensional substorm dynamics, Geophysical Research Letters 22, 2985.

Nagai, T., M. Fujimoto, Y Saito, S. Machida, T. Terasawa, R. Nakamura, T. Yamamoto, T. Mukai, A. Nishida, S. Kokubun (2012), Structure and dynamics of magnetic reconnection for substorm onsets with Geotail observations, Journal of Geophysical Research 103, 4419.

Parker, E. N. (1957), Sweet's mechanism for merging magnetic fields in conducting fuilds, Journal of Geophysical Research 62, 509.

Petschek, H. E. (1964), Physics of Solar Flares, NASA Spec. Pub. 50, 425.

Syrovatskii, S. I. (1971), Formation of current sheets in a plasma with a frozen-in strong magnetic field, Soviet Physics JETP 33, 933.

Sweet, P. A. (1957), Electromagnetic Phenomena in Cosmical Physics, Cambridge U. P., 123.

Wang, X. G., A. Bhattacharjee, Z. W. Ma (2001), Scaling of Collisionless Forced Reconnnection, Physical Review Letters 87, 265003.

Wang, X. G., H. A. Yang, S. P. Jin (2006), Scalings of steady state Hall magnetohydrodynamic reconnection in high-beta plasmas, Physics of Plasmas 13, 060702.

Wang, X. G., Z. W. Ma, A. Bhattacharjee (1996), Fast magnetic reconnection and sudden enhancement of current sheets due to inward boundary flows, Physics of Plasmas 3, 2129.

Xiao, C. J., X. G. Wang, Z. Y. Pu, Z. W. Ma, H. Zhao, G. P. Zhou, J. X. Wang, M. G. Kivelson, S. Y. Fu, Z. X. Liu, Q. G. Zong, M. W. Dunlop, K. H. Glassmeier, E. Lucek, H. Reme, I. Dandouras and C. P. Escoubet (2007), Satellite observations of separator-line geometry of three-dimensional magnetic reconnection, Nature

Physics 3, 609.
Zhang, C. L., Z. W. Ma (2009), Nonlinear evolution of double tearing mode in Hall magnetohydrodynamics, Physics of Plasmas 16, 122113.